IEEE Access
Multidisciplinary | Rapid Review | Open Access Journal

Received May 12, 2020, accepted May 24, 2020, date of publication June 5, 2020, date of current version August 10, 2020.

Digital Object Identifier 10.1109/ACCESS.2020.3000278

Suppression Method for Main-Lobe Interrupted Sampling Repeater Jamming in Distributed Radar

JING CHEN[1], XINLIANG CHEN[2,3], HONGGANG ZHANG[4], KAIXIANG ZHANG[2,3], AND QUANHUA LIU[2,3], (Senior Member, IEEE)

[1]School of Information and Control Engineering, Xi'an University of Architecture and Technology, Xi'an 710055, China
[2]Beijing Key Laboratory of Embedded Real-Time Information Processing Technology, School of Information and Electronics, Beijing Institute of Technology, Beijing 100081, China
[3]Radar Research Laboratory, School of Information and Electronics, Beijing Institute of Technology, Beijing 100081, China
[4]Department of Electronic Engineering, Tsinghua University, Beijing 100084, China

Corresponding author: Xinliang Chen (chenxinliang@bit.edu.cn)

This work was supported by National Natural Science Foundation of China under Grant 61771050, Grant 31727901 and Grant 61625103.

ABSTRACT Main-lobe interrupted-sampling repeater jamming is a coherent type of interference. As this interference is injected through the main lobe of the antenna into a radar system, the interference heavily degrades the performance of the radar system. In this paper, we propose an anti-jamming method based on minimum variance distortionless response (MVDR) that estimates a covariance matrix by obtaining small-sample pure jamming signals through jamming recognition. Time–frequency analysis is performed in the one-dimensional range profile of the pulse-compressed radar echo, and the snapshot sampling of pure jamming is achieved by searching the range gates for the target and the jamming in a two-dimensional range–frequency graph considering the time–frequency differences between the target and jamming signals. Assuming that the available data of snapshot sampling are insufficient, a covariance matrix for pure jamming is reconstructed through an iterative adaptive approach (IAA) and used as the training sample for the MVDR beamformer to suppress main-lobe interrupted-sampling repeater jamming. Finally, the method is validated by comparing the simulation results with the measured results.

INDEX TERMS Main-lobe interrupted-sampling repeater jamming time–frequency analysis, MVDR beamformer.

I. INTRODUCTION

With the growing application of high-speed digital circuit and signal processing in the field of electronic warfare, interrupted-sampling repeater jamming (ISRJ) are becoming important a device. In principle, interrupted-sampling repeater jamming based on DRFM is a process which radar signal is sampled without distortion, the sampled signal is processed properly, and finally reverted to the corresponding simulate signal [1]. A method capable of generating deceptive images from a series of intercepted bistatic chirp pulse is presented [2]. ISRJ based on the digital radio frequency memory (DRFM) technology is a new kind of smart jamming, which aims especially at the linear frequency modulation (LFM) signals with large time bandwidth product [3]. As the ISRJ signals possess the features of radar signals, these signals can obtain the pulse compression gains from radar, which will cause the performance of the radar system to be heavily degraded.

Traditional anti-jamming procedures do not work well when jamming signals are injected into a receiver through the main lobe of a radar antenna. These problems have attracted extensive interest from scientific researchers [4]–[6].

In order to solve the problems caused by interference, some methods of interference suppression have been proposed. First, an active cancelling method using interrupted-sampling and convolution modulation is proposed [7]. Second, according to the differences in the time-frequency-energy domain between the jamming signal and the target echo signal, one method based on the energy function detection and band-pass filtering is proposed [3]. However, these methods rely only on time and frequency resources, resulting that main lobe

The associate editor coordinating the review of this manuscript and approving it for publication was Chengpeng Hao.

interference problem couldn't be completely solved. Because distributed radar can use resources in multiple domains, this article mainly uses it to conduct research.

For distributed array radars which has achieved time-frequency Synchronization [8], main-lobe jamming suppression can be achieved in airspace, time-frequency domain and polarization domain. These methods can only be effective under certain circumstances [9]–[11].

The spatial jamming suppression method is an effective strategy. A null can be formed in the direction of the jamming [12]. The radar cannot obtain pure jamming in the silent state [13]. The jamming suppression method in frequency domain can be divided into two aspects [14]. On the one hands, the radar can have multiple working frequencies to avoid the effects of jamming, on the other hands, the radar can reduce the peak power by using a large time-width bandwidth product signal, reducing the probability of the signal being intercepted by the jammer [15]. At the same time, the energy of the jammer is distributed over a wider frequency band, effectively reducing the jamming distance [16].

In terms of waveform design, anti-jamming can be achieved by designing special waveforms to destroy the output continuity of the Doppler frequency of jamming [17]. In addition, polarization discrimination technology has also become an important method to suppress interrupted-sampling repeater jamming [18].

Apart from passive jamming suppression algorithms described above, jamming recognition can be seen as a proactive approach. Jamming recognition is proactive in anti-jamming efforts by pre-estimating certain jamming parameters for a DRFM jammer, which provides supporting information for method selection, parameter settings, filtering and improvement associated with radar anti-jamming. Thus far, studies of this subject can be separated into two fields: jamming recognition and feature extraction [20].

In the beginning, errors were inevitable in the internal components of a jammer; jamming signals could be effectively identified using the differences between the jamming echo and the target echo in terms of time–frequency domain features. However, as electronic techniques improve, this method is becoming less applicable [19], [20]. For DRFM jamming suppression, a fairly traditional recognition algorithm was used to identify jamming in the time and frequency dimensions through fractional Fourier transform (FRFT) and short-time Fourier transform (STFT) [21]. Jamming signals were distinguished by using the entropy features of the signal when the jammer-to-noise ratio was low [22]. Similarly, inspired by differences in entropy features, the fractal properties of jamming were used to distinguish repeater jamming, and better recognition results were obtained at higher jammer-to-noise ratios [23]. Overall, jamming suppression methods based on jamming recognition are mostly in the initial stage of research, pending a range of further efforts.

In the present study, we try to suppress main-lobe interrupted-sampling repeater jamming by combining a jamming recognition method based on time–frequency features with a space-domain anti jamming algorithm based on large-aperture distributed radar. First, main-lobe jamming suffered by individual radar is transformed into side-lobe jamming for distributed radar through distributed-array radar. Then, the jamming is identified in a one-dimensional range profile through time–frequency feature analysis of the echo signals, and the data of the corresponding range gates can be used as snapshots for pure jamming. For cases where the snapshots for jamming are insufficient, a covariance matrix is reconstructed through an iterative adaptive approach (IAA). Finally, the resulting covariance matrix is applied to the minimum variance distortionless response (MVDR) beamformer to suppress the jamming.

The text is organized as follows. Part I gives a brief outline of the background and current research of main-lobe jamming and interrupted-sampling repeater jamming, along with the overall theme and arrangement of the study; part II describes linearly distributed radar systems, the mathematic modeling of radar signals and interrupted-sampling repeater jamming, and the deficiencies of the traditional space-domain anti-jamming MVDR beamformer; part III elaborates on jamming recognition, beamforming, and the algorithmic principle of IAA; part IV validates the effectiveness of the proposed method by comparing the simulation results and measurement results and examines the anti-jamming performance of the proposed method; part V makes general conclusions.

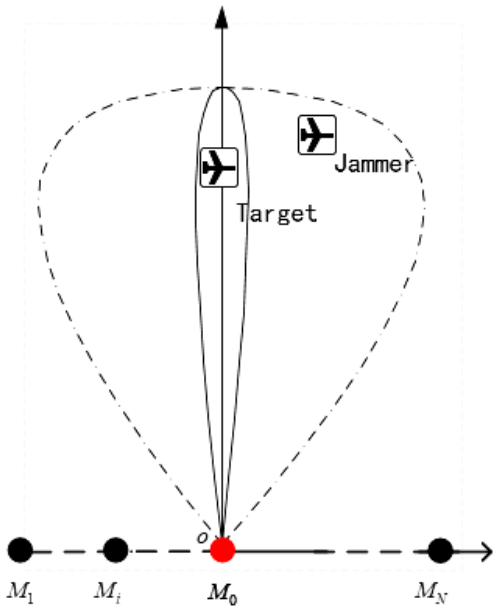

FIGURE 1. Schematic of a distributed radar system.

II. SIGNAL MODEL AND PROBLEM DESCRIPTION

A. SYSTEM

A one-dimensional distributed radar system is composed of one master radar and N number of auxiliary radars, as illustrated by Figure 1. The radar at the phase center at the origin M_0 is the master radar, and $M_1 - M_N$ are the auxiliary radars.

Among the auxiliary radars, $M_1 - M_m$ are on the left side of the master radar, and $M_{m+1} - M_N$ are on the right side of the master radar. It is assumed that the master radar transmits signals to illuminate the target, and the target-reflected signals and the jammer sampling repeater signals are distributed to the individual radars. When master radar operates alone, the beam width is relatively large. The jammer is mounted inside the main lobe, generating main-lobe jamming. A distributed array is produced by adding auxiliary radars. The main lobe then narrows on the synthetic pattern, as illustrated by the dashed line in Figure 1. At this time, the jammer is outside the main lobe in the synthetic pattern of the distributed array, generating side-lobe jamming.

B. SIGNAL MODELING

We assume that the signal transmitted by the radar satisfies Equation (1):

$$s(t) = p(t)\exp(j2\pi f_0 t)\exp(jk\pi t^2) \tag{1}$$

where, t is the time variable, $p(t)$ is the envelope of the transmitted signal, and f_0 is the carrier frequency. When the target or the jammer is far field relative to the distributed array, the steering vectors can be expressed as Equations (2) and (3), respectively:

$$\boldsymbol{a_0} = [\ldots, \exp\{-j2\pi f_0 \frac{id\sin(\theta_0)}{c}\}, \ldots]^{\mathrm{T}} \tag{2}$$

$$\boldsymbol{a_i} = [\ldots, \exp\{-j2\pi f_0 \frac{id\sin(\theta_1)}{c}\}, \ldots]^{\mathrm{T}} \tag{3}$$

In the equations (2) and (3), $i = 0 : N-1$, d is the spacing between the distributed radars, and θ_0 and θ_1 are the spatial angles of the target and the jammer respectively. From Equations (1) and (2), after the target echo is received by the distributed array, the receiving matrix for the baseband signal after frequency conversion can be expressed as Equation (4).

$$\boldsymbol{X}(t) = \boldsymbol{a_0} p\left(t - \frac{2R_0}{c}\right)\exp(-j2\pi f_0 \frac{2R_0}{c}) \exp\left(jk\pi\left(t - \frac{2R_0}{c}\right)^2\right) \tag{4}$$

The target echo signal received by radar $M_i$can be expressed as Equation (5).

$$x_i(t) = p\left(t - \frac{2R_0}{c}\right)\exp(-j2\pi f_0 \frac{2R_0}{c}) \exp\left(jk\pi\left(t - \frac{2R_0}{c}\right)^2\right)\exp\{-j2\pi f_0 \frac{id\sin(\theta_s)}{c}\} \tag{5}$$

In the equation (4) and (5), R_0 is the spacing between the target and the master radar.

Additionally, the DRFM jammer alternately acquires and repeats a sequence of radar signals. This repeating is normally achieved by means such as direct repeating and repetitive repeating. Ignoring the time intervals between the sampling and repeating, the process can be illustrated by the diagrams below.

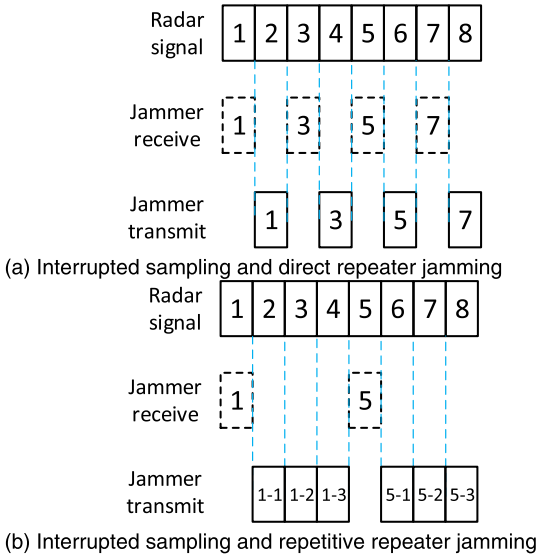

FIGURE 2. Working principle of interrupted sampling repeater jamming.

As shown in these diagrams, the envelope of a direct repeater jamming signal can be expressed by Equation(6).

$$S_{dir}(t) = \sum_{n=0}^{N_c-1} rect\left(\frac{t - \frac{T_J}{2} - (2n+1)T_J}{T_J}\right) S_T(t - T_J) \tag{6}$$

In the equation, T_J is the width of the slice, N_c is the number of slices, and $S_T(t)$ is the envelope of the radar signal intercepted by the jammer [23]. Similarly, the envelope of a repetitive repeater jamming signal can be expressed by Equation(7).

$$S_{rpt}(t) = \sum_{m=1}^{M}\sum_{n=0}^{N_c-1} rect\left(\frac{t - \frac{T_J}{2} - nT_u - mT_J}{T_J}\right) S_T(t - T_J) \tag{7}$$

In the equation, M is the number of repetitions by each slice and $T_u = (m+1)T_J$ is the sampling interval. For repetitive repeater jamming, after the jamming echo is received by the distributed array, the receiving matrix for the baseband signal after the frequency conversion can be expressed by Equation (8)

$$\boldsymbol{Y}(t) = \boldsymbol{a_i} S_{rpt}\left(t - \frac{2R'}{c}\right) \tag{8}$$

The jamming signal received by radar M_i can be expressed as Equation(9).

$$y_i(t) = S_{rpt}\left(t - \frac{2R'}{c}\right)\exp\{-j2\pi f_0 \frac{id\sin(\theta_i)}{c}\} \tag{9}$$

In the equation, R' is the spacing between the master radar and the jammer and θ_i is the direction of the jammer.

C. PROBLEM DESCRIPTION

The interrupted-sampling repeater jamming is generated by the DRFM jammer, which first intercepts the signals transmitted by the radar, samples one segment and repeats the segment, then samples the next segment and repeats the segment until the end of the radar pulse. As the interrupted-sampling repeater jamming signals possess the features of radar signals, these signals can obtain the pulse compression gains from radar such that the target signals are submerged in a dense decoy target group.

Traditional space-domain anti-jamming procedures use the spatial dispersion of the target and the jammer to provide gains for the signals along the target direction and suppress the signals along the direction of the jammer. However, as a DRFM jammer stops sampling after the radar stops working, it is impossible for radar to obtain pure jamming signals in a passive way. The target information is contained in the training data for anti-jamming treatment. In space-domain adaptive signal processing, when the direction of arrival (DOA) is established, the jamming signals can be suppressed, and the target signals can be retained regardless of whether the target signals are contained in the training data. Unfortunately, in practical applications, it is generally impossible to obtain the exact DOA. When there is an estimation error in the DOA, if the target signals are not contained in the training data, the jamming signals can be suppressed by anti-jamming procedures with minimal losses in the target signal; if the target signals are contained in the training data, the jamming signals can still be suppressed by anti-jamming procedures but with considerable losses in the target signal. The higher the intensity of the target signal is, the greater the loss of the target signal is. Hence, when there is an estimation error in the DOA, traditional space-domain adaptive anti-jamming approaches are challenged by serious signal cancellation [24], [25].

III. JAMMING SUPPRESSION METHOD BASED ON JAMMING RECOGNITION

A. JAMMING RECOGNITION METHOD BASED ON TIME-FREQUENCY ANALYSIS OF ONE-DIMENSIONAL RANGE PROFILES

We assume that direct interrupted-sampling repeater jamming is generated by the jammer. The signal received by radar M_i in the distributed radar system can be expressed as:

$$\begin{aligned} & s_i(t) \\ & = A_x x_i + A_y y_i + n_0(t) \\ & = A_x \mathrm{rect}\left(\frac{t-\frac{T}{2}-\tau_x}{T}\right)\exp(jk\pi(t-\tau_x)^2) \\ & \quad \exp(-j2\pi f_0\tau_x) + A_y \sum_{n=0}^{N_c-1} \mathrm{rect}\left(\frac{t-\frac{T_J}{2}-(2n+1)T_J-\tau_y}{T_J}\right) \\ & \quad \exp(jk\pi(t-T_J-\tau_y)^2)\exp\left[-j2\pi f_0(T_J+\tau_y)\right] + n_0(t) \end{aligned} \tag{10}$$

In Equation(10), $A_x x_i$ is the target component received by the radar, $A_y y_i$ is the jamming component received by the radar, $n_0(t)$ is the receiver noise of the radar; T is the pulse width of the linear frequency modulation (LFM) signal transmitted by the radar, A_x and A_y are the amplitudes of the target and jamming signals before pulse compression, respectively, and τ_x and τ_y are the round-trip delays of the target and the jammer relative to radar M_i, respectively, expressed by Equations (11) and(12).

$$\tau_x = \frac{2R_0}{c} + \frac{id\sin(\theta_0)}{c} \tag{11}$$

$$\tau_y = \frac{2R_i}{c} + \frac{id\sin(\theta_i)}{c} \tag{12}$$

The one-dimensional range profile from pulse compression of the received signal can be expressed as Equation (13).

$$\begin{aligned} S_{\mathrm{pc}}(t) = {} & A_x' \sin \mathrm{c}[kT(t-\tau_x)]exp[-jk\pi(t-\tau_x)^2] \\ & + A_x' \sin \mathrm{c}\left[kT_J(t-T_J-\tau_y)\right] \\ & \exp[-jk\pi(t-T_y-\tau_y)^2]\frac{1-\exp(2jN_y\phi)}{1-\exp(2j\phi)} + n_1(t) \end{aligned} \tag{13}$$

In the equation, $\phi = 2\pi kT_J(t-T_J-\tau_y)$, A_x and A_y are the amplitudes of the target and the jamming signals after pulse compression, respectively, the first term represents the pulse compression result for the target echo, the second term represents the pulse compression result of the jamming signal, and $n_1(t)$ represents the pulse compression result of the noise term. The amplitude response of the pulse compression result of the jamming is described by Equation(14).

$$\left|S_{PC\_Y}\right| = \left|A_y' \sin \mathbf{c}\left[kT_J(t-T_J-\tau_y)\right]\frac{\sin(N_c\phi)}{\sin(\phi)}\right| \tag{14}$$

From this equation, on the one-dimensional range profile, the jamming comprises one primary decoy target and a number of symmetrically distributed secondary decoy targets, which as a whole conform to the sinc envelope [26]. Given that the envelope term is $\mathrm{sinc}[kT_J(t-T_J-\tau_y)]$, the width of the main lobe is $2/kT_J$. If each slice repeats M times, the interval between adjacent targets is $\Delta t = 1/(M+1)\,T_J$. Then, the number of jamming peaks in the main lobe of the jamming after pulse compression is:

$$Num = \frac{2/kT_J}{\Delta t} - 1 = 2M + 1 \tag{15}$$

Time–frequency analysis is performed on the pulse-compressed one-dimensional range profile:

$$TF(\tau, f) = \int_{-\infty}^{\infty} \mathrm{rect}\left(\frac{t-\tau}{T_w}\right) S_{pc}(t)\exp(-j2\pi ft)dt \tag{16}$$

In this way, the two-dimensional range–frequency graph is obtained. In the range dimension, the target and the jammer are located in different range gates; in the frequency dimension, as the envelope of the target signal is a standard

sinc function after pulse compression, and the main-lobe width of this sinc function is the reciprocal of the bandwidth, after fast Fourier transform (FFT), the spectrum of this main lobe, which corresponds to the bandwidth of the LFM signal, appears on the time–frequency graph as a line on the frequency dimension, and the length of this line represents the bandwidth of the signal. The pulse compression result of the jamming signal, on the other side, is composed of a number of slices stacked together. As the slices are very limited in width, in the time–frequency graph, the width of the signal is obviously smaller than that of the target in the frequency dimension. Additionally, as different inception points result in different initial phases, the time-frequency analysis results of the jamming correspond to different bands in the frequency domain. Using this feature difference, it is possible to recognize the target from the jamming and discriminate the time-domain range gates for the target and the jammer [27], [28].

The following target–jamming recognition procedure is used:

Step 1: In the initialization stage, we establish a two-dimensional range–frequency window. The window length of the range profile is the main-lobe width of the target after pulse compression and remains constant, and that of the starting frequency profile is 1; the starting position of the range profile is 0m, and the starting point of the frequency profile is $-B/2$Hz;

Step 2: We determine the distance range between the target and the interference. First, we fix the frequency dimension so that the window glides in the range dimension and record the mean amplitude in the window at the same time. When the mean amplitude increases or decreases progressively, we can determine whether there is a target or jammer in this range gate.

Step 3: We judge the signal in the frequency dimension. After completing Step 2, we fix the range dimension, extend the length of the frequency window and record the maximum amplitude of the frequency dimension. If the variation amplitude is smaller than η_1 within $-B/2\text{Hz} \sim B/2\text{Hz}$, the frequency dimension is assumed to be continuous, and this range gate is the target; if the variation amplitude at certain frequency points is greater than η_2 within $-B/2\text{Hz} \sim B/2\text{Hz}$, the frequency dimension is assumed to be discontinuous, and this range gate is the jamming. We record the range gate information for the target and the jammer.

We perform Steps 1 through 3 on the two-dimensional time–frequency analysis graphs of the echoes from individual channels. Among the jamming data from these channels, the data of jamming that share the same or similar jamming range gates can be used as the same group of sampling snapshots, whereas the data of those with significantly different jamming range gates are discarded. If the jamming range gates for the channels are significantly different, Steps 1 through 3 may be performed again until a group of sampling snapshots is obtained.

B. JAMMING SUPPRESSION BASED ON IAA

According to the jamming recognition and range gate discrimination results, a set of data corresponding to high effective peaks in the main lobe of the jamming in the one-dimensional range profile is extracted to constitute training data $\boldsymbol{X}$, which represents an estimate of pure jamming signals and does not contain the target signal. Theoretically, the use of this training data helps avoid the signal cancellation problems challenging traditional adaptive filter regimes. Using the training data, the covariance matrix can be estimated by Equation(17).

$$\boldsymbol{R}_{\boldsymbol{X}} = (\boldsymbol{X}\boldsymbol{X}^{\mathrm{H}})/L \tag{17}$$

In the equation, insufficient sampling points are yielded by jamming recognition, the resulting covariance matrix may not be very accurate, and the anti-jamming performance may not be sufficient as a consequence. Traditionally, a covariance matrix is reconstructed by DOA estimation using a Capon spatial spectrum [29]–[31]. When IAA is used for reconstruction, DOA estimation is omitted, and the estimation is more stable in the presence of coherent interference and estimation errors for the desired signal directions [32]–[34].

We define $\boldsymbol{A}(\theta) \triangleq [\boldsymbol{a}_1\ \boldsymbol{a}_2\ \ldots\ \boldsymbol{a}_k]$, where $\boldsymbol{a}_k$ represents the steering vector of the$k$th space angle; the envelope of each angle is $s(n) \triangleq [s_1(n)\ s_2(n)\ \ldots\ s_K(n)]^T$. The IAA procedure is performed as follows:

$$\hat{s}_k(n) = \boldsymbol{a}_k^{\mathrm{H}}\boldsymbol{y}(n)/M, \quad n = 1, \ldots, N,\ k = 1, \ldots, K \tag{18}$$

$$P_k = \frac{1}{N}\sum_{n=1}^{N}\left|\hat{s}_k(n)\right|^2, \quad k = 1, \ldots, K \tag{19}$$

$$\overline{\boldsymbol{R}} = \boldsymbol{A}(\theta)\boldsymbol{P}\boldsymbol{A}^{\mathrm{H}}(\theta) \tag{20}$$

The iteration process can be expressed as follows:

$$\begin{cases} \boldsymbol{w}_k = \dfrac{\boldsymbol{R}^{-1}\boldsymbol{a}_k}{\boldsymbol{a}_k^{\mathrm{H}}\boldsymbol{R}^{-1}\boldsymbol{a}_k} \\ P_k = \boldsymbol{w}_k^{\mathrm{H}}\boldsymbol{R}\boldsymbol{w}_k \end{cases} \tag{21}$$

where $k = 1, \ldots, K$ is the number of iterations.

The iteration ends when the relative variation $\left|\hat{s}_k^{(i)} - \hat{s}_k^{(i-1)}\right|^2$ of the ith iteration is smaller than the prescribed error limit.

The covariance matrix for jamming plus noise can be expressed as:

$$\boldsymbol{R}_{i+n} = \int_{\overline{\Theta}} P_{capon}(\theta)\boldsymbol{a}(\theta)\boldsymbol{a}^{\mathrm{H}}(\theta)d\theta \tag{22}$$

Here, $P(\theta)$ is the estimate by the Capon spatial spectrum. $\overline{\Theta}$ is the desired angle for the signal, which can be determined by the IAA spatial spectrum. Hence, the covariance matrix reconstructed for jamming plus noise can be expressed as:

$$\boldsymbol{R}_{i+n} = \sum_{\theta_k \in \overline{\Theta}} P_k\boldsymbol{a}(\theta_k)\boldsymbol{a}^{\mathrm{H}}(\theta_k) \tag{23}$$

For the MVDR beamformer, under constant gains in the target azimuth and the minimal total output power, the optimal weight vector can be expressed by Equation(24).

$$\boldsymbol{W_{opt}} = P_{out,\max}\boldsymbol{R}_X^{-1}\boldsymbol{a_0} \tag{24}$$

In the equation, $P_{out,\max} = \left[\boldsymbol{a_0}^{\mathrm{H}}\boldsymbol{R}_X^{-1}\boldsymbol{a_0}\right]^{-1}$ is the minimal output power corresponding to the optimal weight vector, and $\boldsymbol{a_0}$ is the steering vector of the target direction. The jamming can be suppressed by using the weight vector in this equation against the received signals [35].

IV. SIMULATION

This section verifies the proposed algorithm through three parts. Part A illustrates that the algorithm is effective for the two DRFMs mentioned in Section II.B. Part B illustrates the effect of changes in scene parameters (such as INR, SNR, estimation error of the DOA, direction of the jammer) on the algorithm performance. Besides these results of simulation experiments in both Part A and Part B, we use the real data received by radar to illustrate the feasibility of the method in Part C.

Simulation conditions: A ''one master radar, four auxiliary radars'' linear distributed radar array is established with radars evenly distributed at 10m intervals among the radars. The beams are oriented in the normal direction. The radar signal parameters are listed below:

TABLE 1. This is a table. Tables should be placed in the main text near to the first time they are cited.

Parameter	Value	Parameter	Value
Center frequency (GHz)	1	Signal bandwidth (MHz)	10
Sampling frequency (MHz)	80	Pulse width (μs)	20
η_1 (dB)	4	η_2 (dB)	12

A. VALIDATION OF THE PROPOSED METHOD

As the signals are instantaneous narrowband signals, and the target and jamming satisfy far-field conditions relative to the distributed array, based on the wave plane model, there are the following groups of simulations:

Simulation 1: We assume that the target is in the normal direction, the angle between the direction of the jammer and the direction of the target is 0.5°, and the estimation error of the DOA is 0.2°; the jamming is a direct interrupted-sampling repeater jamming type with slice width of 2.5μs and involves four slices, each repeating one time; the signal-to-noise ratio (SNR) is 0dB, and the interference-to-noise ratio (INR) is 40dB. Three sampling snapshots are obtained through jamming recognition. On this basis, the jamming is suppressed through IAA.

Simulation 2: We assume that the target is in the normal direction, the angle between the direction of the jammer and the direction of the target is 0.5°, and the estimation error of the DOA is 0.2°; the jamming is a repetitive repeater jamming with a slice width of 2.5μs and involves two slices, each repeating three times; the SNR is 0dB, and the INR is 40dB. Three sampling snapshots are obtained through jamming recognition. On this basis, the jamming is suppressed through IAA.

When evaluating the anti-jamming performance, the loss of SNR is defined as the difference between the echo SNR after anti-jamming treatment and that before treatment. The signal to interference-plus-noise ratio (SINR) improvement represents the improvement of the SINR after anti-jamming treatment relative to that before this treatment; $SNR = \sigma_s^2/\sigma_n^2$, and $SINR = \sigma_s^2/(\sigma_i^2 + \sigma_n^2)$, where σ_s^2, σ_i^2, and σ_n^2 are the powers of the target, jamming, and noise, respectively.

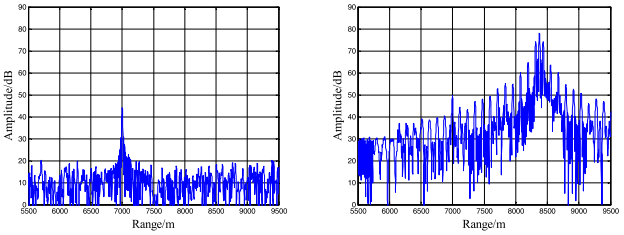

(a) (b)

(a) Pulse-compressed one-dimensional range profile of the target echo
(b) Pulse-compressed one-dimensional range profile of the target-plus-jamming echo

FIGURE 3. One-dimensional range profiles of the target and the direct repeater jamming.

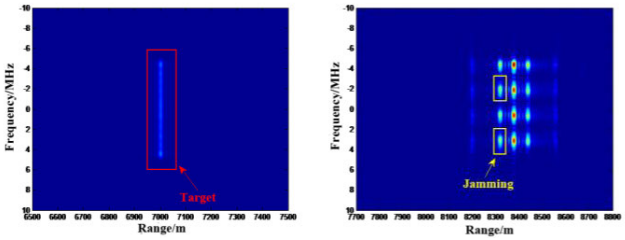

(a) (b)

(a) Result of target recognition (b) Result of jamming recognition

FIGURE 4. Results of target and jamming recognition based on two-dimensional range–frequency graph.

Figure 3(a) shows the one-dimensional range profile of the target echo after pulse compression. Figure 3(b) shows the pulse-compressed one-dimensional range profile of the target-plus-jamming echo. The time–frequency analysis of these profiles is given in Figure 4. According to the discussions in section III.B, in the two-dimensional time–frequency graphs of the one-dimensional range profiles, the target and the jamming are in different range gates; the target is continuously distributed in the frequency dimension, and its length approximates the bandwidth; the jamming is discontinuously distributed in the frequency dimension. In a two-dimensional range–frequency window, it is possible to recognize the target and the jamming by gliding along the range dimension to observe the variation in the amplitude of the range dimension

and examining the frequency dimension. An enlarged view of the range gate for the target is shown in Figure 4(a). An enlarged view of the range gate for the jamming decoy target group is shown in Figure 4(b).

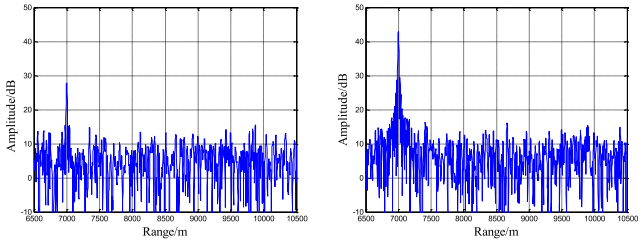

(a) Anti-jamming results by the traditional method
(b) Anti-jamming results by the proposed method

FIGURE 5. Pulse compression results after the anti-jamming treatment.

Figure 5(a) shows the pulse-compressed one-dimensional range profile after anti-jamming treatment by the traditional method. When there is estimation error in the DOA, the traditional method suffers a loss in the target signal, although this method does suppress the jamming. A closer analysis reveals a loss of 12.5dB in the SNR and a jamming residual of 0.55dB. Figure 5(b) shows the pulse-compressed one-dimensional range profile after anti-jamming treatment by the proposed method. When the covariance matrix is estimated with three or more jamming sampling snapshots obtained through jamming recognition, it is possible to suppress direct repeater jamming and retain the target signals well. A closer analysis reveals a loss of 1.4dB in the SNR and a jamming residual of 0.75dB.

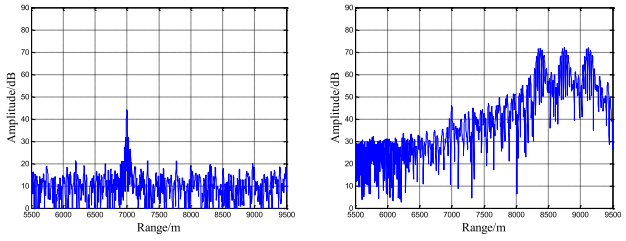

(a) Pulse-compressed one-dimensional range profile of the target echo
(b) Pulse-compressed one-dimensional range profile of the target-plus-jamming echo

FIGURE 6. One-dimensional range profiles of the target and the repetitive repeater jamming.

Figure 6(a) shows the one-dimensional range profile of the target echo after pulse compression. Figure 6(b) shows the one-dimensional range profile of the target-plus-jamming echo after pulse compression. The time–frequency analysis of these graphs is given in Figure 4. Figure 7(a) shows the results of the target recognition. Figure 7(b) shows the results of the jamming recognition. An enlarged view of the range gate of the target is given in Figure 7(a). An enlarged

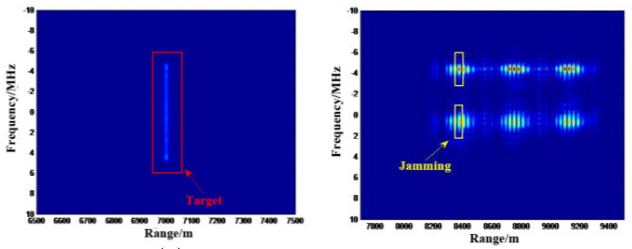

(a) Result of target recognition (b) Result of jamming recognition

FIGURE 7. Results of target and jamming recognition based on two-dimensional range–frequency graphs.

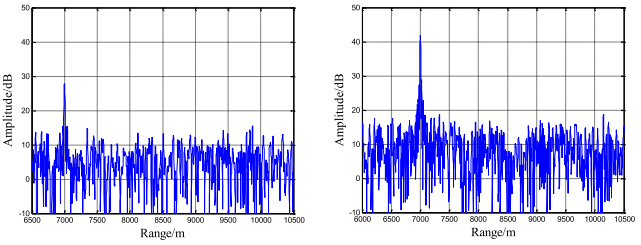

(a) Anti-jamming result by the traditional method
(b) Anti-jamming result by the proposed method

FIGURE 8. Pulse compression results after anti-jamming treatment.

view of the range gate of the jamming decoy target group is given in Figure 7(b). Figure 8(a) shows the pulse-compressed one-dimensional range profile after anti-jamming treatment by the traditional method. When there is estimation error in the DOA, the traditional method suffers a loss in the target signal, although this method does suppress the jamming. A closer analysis reveals a loss of 14.1dB in the SNR and a jamming residual of 0.42dB. Figure 8(b) shows the pulse-compressed one-dimensional range profile after anti-jamming treatment by the proposed method. When the covariance matrix is estimated with three or more jamming sampling snapshots obtained through jamming recognition, it is possible to suppress direct repeater jamming and retain the target signals well. A closer analysis reveals a loss of 1.0dB in the SNR and a jamming residual of 0.67dB.

Simulation 3: We assume that the target is in the normal direction, the angle between the direction of the jammer and the direction of the target is 0.5°, and the jamming pattern and parameters are the same as those in Simulation 1 the angle between the estimated desired signal direction and the real target direction is 0.2°; the INR is 40dB; one sampling snapshot is obtained through jamming recognition. On this basis, the jamming is suppressed through IAA.

As illustrated in Figure 9(a), when only one jamming sampling snapshot is available, it is impossible to effectively cancel the jamming. However, with this same sampling snapshot, when IAA is used to reconstruct the covariance matrix and anti-jamming treatment is performed, the result is as given in Figure 9(b). A closer analysis reveals a loss of 0.93dB in the SNR and a jamming residual of 1.35dB.

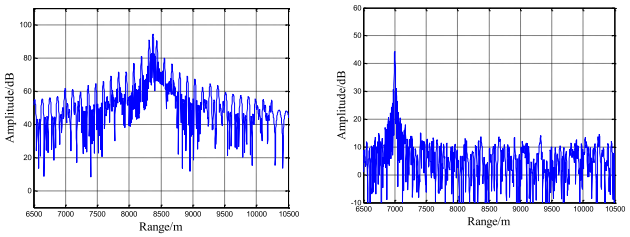

(a) Anti-jamming result by single sampling snapshot
(b) Anti-jamming result by single sampling snapshot based on IAA

FIGURE 9. Pulse compression results after anti-jamming treatment.

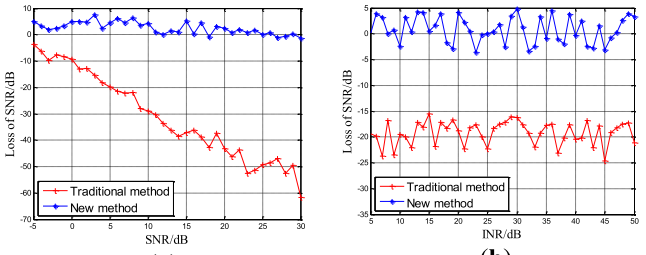

(a) Loss of SNR versus SNR
(b) Loss of SNR versus INR

FIGURE 11. Anti-jamming performance of the proposed method versus that of the traditional method.

B. ANTI-JAMMING PERFORMANCE OF THE PROPOSED METHOD

Simulation 4: effect of INR on the rate of recognition

We assume that the target is in the normal direction, the angle between the direction of the jammer and the direction of the target is 0.5°, and the jamming pattern and parameters are the same as those in Simulation 1.

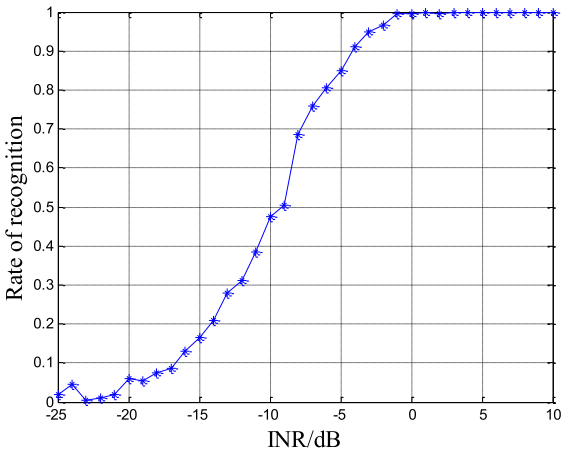

FIGURE 10. INR versus the rate of jamming recognition.

As illustrated by Figure 10, when the INR before pulse compression is low, the jamming signal is lower than the noise level, and the rate of jamming recognition is almost zero. As the INR increases, so does the rate of recognition; at INR $= -10$dB, the rate of recognition is 50%, and at INR $= -4$dB, the rate of recognition is as high as 90%.

Simulation 5: effect of SNR and INR on loss of SNR

We assume that the target is in the normal direction, the angle between the direction of the jammer and the direction of the target is 0.5°, the jamming pattern and parameters are the same as those in Simulation 1, and the SNR is 0dB. The angle between the estimated desired signal direction and the real target direction is 0.2°. The loss of SNR as a function of the INR of the jamming signal obtained by the proposed method is quantitatively compared with that obtained by the traditional method. We assume that only one sampling snapshot is obtained through jamming recognition. Adaptive jamming cancellation is performed by reconstructing a covariance matrix through IAA.

As illustrated by Figure 11(a), when there is estimation error in the DOA, the traditional anti-jamming method suffers a considerable loss of SNR since the training samples of this method contain target information, and this loss increases with the radar signal SNR. The proposed method displays a smaller loss of SNR since the samples of this method do not contain target information, and this method is particularly effective in cases of high SNR. As illustrated by Figure 11(b), under a fixed SNR and a fixed deviation in the estimated desired signal direction, as INR varies, the loss of SNR after anti-jamming treatment by the traditional method is greater than that by the proposed method.

Simulation 6: effect of estimation error of DOA on loss of SNR and improvement of SINR

We assume that the target is in the normal direction, the angle between the direction of the jammer and the direction of the target is 0.5°; the direct repeater jamming is generated by the jammer, and the jamming pattern and parameters are the same as those in Simulation 1; the SNR is 0dB, and the INR is 40dB; the estimation error of the DOA varies from $-5°$ to 5°. The loss in the SNR and the improvement in the SINR as functions of the estimation error of DOA obtained by the proposed method are quantitatively compared with those obtained by the traditional method. We assume that only one sampling snapshot is obtained. The anti-jamming treatment is performed by reconstructing a covariance matrix through IAA.

As illustrated by Figure 12(a), when there is no estimation error in the DOA, the loss of SNR is close to 0 dB for both the traditional method and the proposed method. As the estimation error in the DOA increases, the traditional method suffers a considerable loss of SNR for almost all deviated angles except for certain particular angles, whereas the proposed method has only a very small loss in the SNR when there is estimation error in the DOA. Similarly, as illustrated by Figure 12(b), when there is estimation error in the DOA, the traditional method provides minimal improvement in the SINR, whereas the proposed method is able to provide a level of improvement in the SINR.

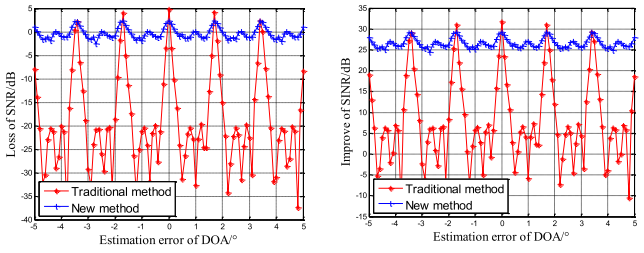

(a) (b)

(a) Loss of SNR versus estimation error of DOA
(b) Improvement of SINR versus estimation error of DOA

FIGURE 12. **Anti-jamming performances by the proposed method versus the traditional method.**

Simulation 7: effect of the direction of the jammer on loss of SNR

We assume that the target is in the normal direction, the direction of the jammer traverses from $-5°$ to $5°$, the jamming pattern and parameters are the same as those in Simulation 1, the SNR is 0dB, and the INR is 40dB; the angle between the estimated desired signal direction and the real target direction is $0.2°$. The loss of SNR as a function of the INR of the jamming signal obtained by the proposed method is compared with that obtained by the traditional method.

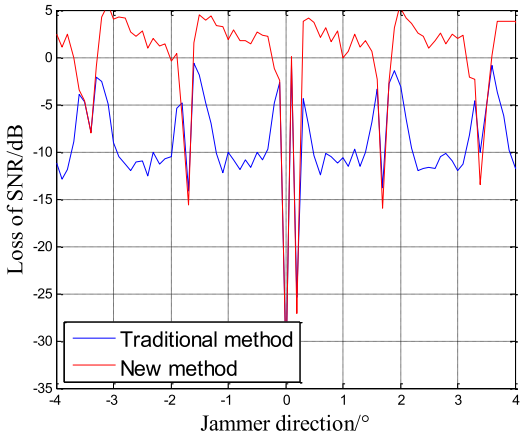

FIGURE 13. **Loss of SNR versus the direction of the jammer.**

A large number of grating lobes exist in the direction pattern of the large-aperture distributed radar. If the jamming is located at the grating lobe, when adaptive anti-jamming treatment is performed, the presence of grating zeros results in energy damage to the target. According to the array parameters, the grating lobe angles are $-1.71°$, $0°$, $1.71°$, and $3.42°$. As illustrated by Figure 13, when the jamming is at a nongrating lobe angle, the loss of SNR from the proposed method is much smaller than that by the traditional method; however, when the jamming is at a grating lobe angle, both the proposed method and the traditional method suffer great loss of SNR. The same phenomenon occurs when the direction of the jammer coincides with the estimated desired signal angle.

C. MEASUREMENT RESULTS

A "one master, two Auxiliary radars" one-dimensional nonuniform sparse array is constructed. The system works in the S waveband; the aperture of the unit array is 0.5m, and the array baseline is 3.5m. Consequently, the unit array beam width is approximately $10.4°$, and the synthetic beam width of the distributed array is approximately $1.46°$; the angle between the jammer and the target is $3.2°$; the jamming is a repetitive repeater jamming, with each slice repeating two times. The pulse compression results of the raw echo are given in the graphs below.

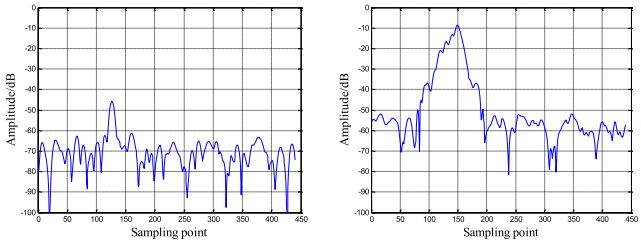

(a) (b)

(a) Pulse compression results of the target echo
(b) Pulse compression results of the target-plus-jamming echo

FIGURE 14. **Pulse compression results of the raw signal echo.**

When the traditional MVDR adaptive anti-jamming method is used, adaptive treatment is performed using a covariance matrix estimated with the target-plus-jamming echo data. Cases where the steering vector is correctly estimated and where this vector is incorrectly estimated are considered. In the latter case, the estimation error in the DOA is $0.4°$. The results are given in the graphs below.

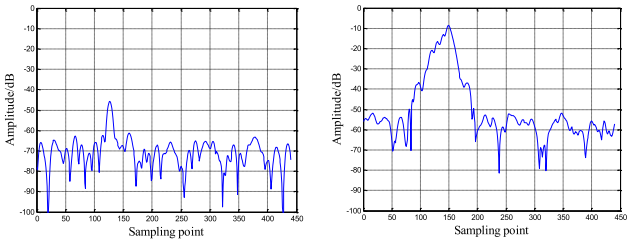

(a) (b)

(a) Steering vector correctly estimated
(b) Steering vector incorrectly estimated (estimation error in the DOA is 0.4°)

FIGURE 15. **Pulse compression results by the traditional time-domain MVDR beamforming method.**

Figure 15(a) shows the anti-jamming results when the steering vector of the target direction is correct, where the loss in the SNR is 1.32dB. Figure 15(b) shows the anti-jamming results when the steering vector of the target direction is incorrect, where the loss of SNR is 10.53dB. Greater energy losses occur in the target signal when the steering vector of the target direction is incorrectly estimated.

Assuming that the steering vector of the target direction is incorrect, the proposed anti-jamming method is used.

Data from one of the jamming sampling points shown in Figure 14(b) are taken and treated in two different procedures. In the first procedure, adaptive treatment is performed by directly estimating a covar iance matrix on the basis of one jamming sampling point. In the second procedure, adaptive treatment is performed by reconstructing a covariance matrix with data from one jamming point after IAA treatment. The results are given in the graphs below.

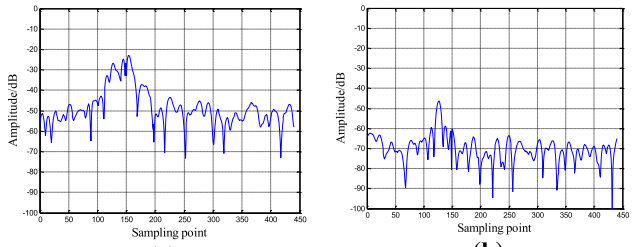

(a) Cancellation results using covariance estimated with one sampling point
(b) Cancellation results using covariance estimated with one sampling point and performing IAA

FIGURE 16. Pulse compression results by the proposed time-domain MVDR anti-jamming method.

Figure 16(a) shows the pulse compression results by directly estimating a covariance with data from one single jamming sampling point and performing IAA. From these graphs, if samples are trained with a covariance estimated with the data from a single jamming sampling point, it is impossible to effectively suppress the jamming; if the samples are trained with a covariance reconstructed through IAA, it is possible to suppress the jamming when the steering vector of the target is incorrect, with a loss of 1.74dB in the SNR, which is better than that obtained by the traditional method.

Figure 17 compares the loss in the SNR obtained by the traditional method and that obtained by the proposed method in cases where the steering vector is incorrectly estimated and the deviated angle traverses from $-0.75°$ to $0.75°$.

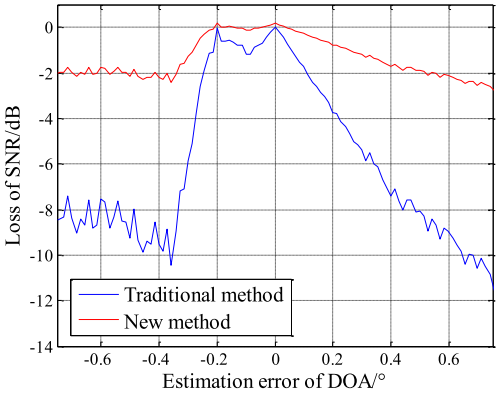

FIGURE 17. Loss of SNR versus estimation error of DOA.

From this graph, when the steering vector of the target is incorrect, the traditional time-domain MVDR beamforming method suffers a considerable loss of SNR, and the proposed method is subject to a lower loss of SNR.

V. CONCLUSIONS

Main-lobe jamming and interrupted-sampling repeater jamming are potential threats to the normal operation of monostatic radar systems. When a large-aperture distributed radar system is constructed, while space-domain adaptive anti-jamming procedures can suppress main-lobe interrupted-sampling repeater jamming, these method are inevitably challenged by signal cancellation resulting from the estimation error of the DOA. In the present study, we try to obtain jamming sampling snapshots by recognizing jamming decoy targets in a one-dimensional range profile by using a method that compounds the jamming recognition method based on time–frequency analysis of one-dimensional range profiles with the distributed space-domain anti-jamming method. As insufficient snapshots for jamming are obtained, a covariance matrix is reconstructed through IAA on the basis of these snapshots for jamming, and the adaptive anti-jamming treatment is performed thereafter. The results demonstrate that in addition to effectively suppressing the jamming, the proposed method is able to limit signal losses to a certain extent. Comparison between simulation results and measurements confirms that the proposed method outperforms the traditional method for both interrupted sampling and direct repeater jamming and interrupted sampling and repetitive repeater jamming; when there is estimation error in the DOA, this method suffers a lower loss in the SNR and provides a greater improvement in the SINR after anti-jamming treatment.

REFERENCES

[1] X. Wang, J. C. Liu, W. Zhang, Q. X. Fu, Z. Liu, and X. Xie, "Mathematic principles of interrupted-sampling repeater jamming (ISRJ)," *Sci. China*, vol. 1, pp. 115–125, Feb. 2007.
[2] X. Pan, D. Feng, Q. Fu, W. Wang, Y. Liu, and G. Wang, "On deception jamming for countering bistatic ISAR based on sub-nyquist sampling," *IET Radar, Sonar Navigat.*, vol. 8, no. 3, pp. 173–179, Mar. 2014.
[3] H. Yuan, C.-Y. Wang, X. Li, and L. An, "A method against interrupted-sampling repeater jamming based on energy function detection and band-pass filtering," *Int. J. Antennas Propag.*, vol. 2017, pp. 1–9, Mar. 2017.
[4] T. Long, H. Zhang, T. Zeng, X. Chen, Q. Liu, and L. Zheng, "Target tracking using SePDAF under ambiguous angles for distributed array radar," *Sensors*, vol. 16, no. 9, p. 1456, Sep. 2016.
[5] C. Zhou, F. Liu, and Q. Liu, "An adaptive transmitting scheme for interrupted sampling repeater jamming suppression," *Sensors*, vol. 17, p. 2480, Nov. 2017.
[6] T. Long, Z. Liang, and Q. Liu, "Advanced technology of high-resolution radar: Target detection, tracking, imaging, and recognition," *Sci. China Inf. Sci.*, vol. 62, no. 4, pp. 5–30, Apr. 2019.
[7] Q. Huang and Y. Xu, "Active cancellation stealth analysis based on interrupted-sampling and convolution modulation," *Optik*, vol. 127, no. 7, pp. 3499–3503, Apr. 2016.
[8] L. Wang, "High precision synchronization of time and frequency and its applications," *Physics*, vol. 43, no. 6, pp. 360–363, 2014.
[9] L. Ning and X. Yang, "Multi-base polarization radar main-lobe interference suppression algorithm," *J. Signal Process.*, vol. 33, no. 12, pp. 1571–1577, Dec. 2017.
[10] J. Ma, L. Shi, Y. Li, S. Xiao, and X. Wang, "Angle estimation of extended targets in main-lobe interference with polarization filtering," *IEEE Trans. Aerosp. Electron. Syst.*, vol. 53, no. 1, pp. 169–189, Feb. 2017.

[11] D. Wu, Z. Xu, L. Zhang, Z. Xiong, and S. Xiao, "Performance analysis of polarization-space-time three-domain joint processing for clutter suppression in airborne radar," *Prog. Electromagn. Res.*, vol. 129, no. 7, pp. 579–601, Jul. 2012.
[12] L. Yu, X. Zhang, and Y. Wei, "Adaptive beamforming technique for large-scale arrays with various subarray selections," in *Proc. CIE Int. Conf. Radar (RADAR)*, Guangzhou, China, Oct. 2016, pp. 1–4.
[13] F. A. Butt and M. Jalal, "An overview of electronic warfare in radar systems," in *Proc. Int. Conf. (TAEECH)*, 2013, pp. 213–217.
[14] S. Bidon, J. Y. Tourneret, and L. Savy, "Bayesian sparse estimation of migrating targets for wideband radar," *IEEE Trans. Aerosp. Electron. Syst.*, vol. 50, no. 2, pp. 817–886, Apr. 2014.
[15] Y. D. Shriman, V. M. Orlenko, and S. P. Leshchenko, "Advantages and problems of wideband radar," in *Proc. Int. Conf. Radar*, 2003, pp. 15–21.
[16] F. L. Chevalier, "Future concepts for electromagnetic detection: From space-time-frequency resources management to wideband radars," *IEEE Aerosp. Electron. Syst. Mag.*, vol. 14, no. 10, pp. 9–17, 1999.
[17] S. Chang, H. Zhang, T. Long, Q. Liu, and L. Zheng, "A radar waveform bandwidth selection strategy for wideband tracking," *Sci. China Inf. Sci.*, vol. 62, no. 4, p. 40306, Apr. 2019.
[18] L. Song, X. Qiao, and X. Meng, "Study on the method of polarization suppression of cheating jamming in pulse Doppler radar," *J. Syst. Eng. Electron.*, vol. 16, no. 2, pp. 310–315, 2005.
[19] A. Marino, S. R. Cloude, and I. H. Woodhouse, "A polarimetric target detector using the Huynen fork," *IEEE Trans. Geosci. Remote Sens.*, vol. 48, no. 5, pp. 2357–2366, May 2010.
[20] D. Orlando, "A novel noise jamming detection algorithm for radar applications," *IEEE Signal Process. Lett.*, vol. 24, no. 2, pp. 120–206, Feb. 2017.
[21] C. Zhou, Q. Liu, and X. Chen, "Parameter estimation and suppression for DRFM-based interrupted sampling repeater jammer," *IET Radar, Sonar Navigat.*, vol. 12, no. 1, pp. 56–63, Jan. 2018.
[22] M. Greco, F. Gint, and A. Farina, "Radar detection and classification of jamming signals based on cone classes," *IEEE Trans. Signal Process.*, vol. 56, no. 5, pp. 1984–1993, Jan. 2008.
[23] P. C. J. Hill and V. Truffert, "Statistical processing techniques for detecting DRFM repeat-jam radar signals," in *Proc. IEE Colloq. Signal Process. Techn. Electron. Warefare*, 1992, pp. 1–6.
[24] F. Wang, Z. Lei, and Q. Chen, "Repeat jamming cognition using time-frequency chips in u-domain," *Chin. J. Radar Sci.*, vol. 29, no. 2, pp. 358–362, Feb. 2014.
[25] F. Shi, C. Zhou, and Q. Liu, "Characteristics analysis of interrupted-sampling repeater jamming," (in Chinese), *J. Signal Process.*, vol. 33, no. 12, pp. 1616–1624, Dec. 2017.
[26] Y. Wang, Q. Ding, and R. Li, *Adaptive Array Processing*. Beijing, China: Tsinghua Univ. Press, 2009, pp. 30–43.
[27] R. G. Lorenz and S. P. Boyd, "Robust minimum variance beamforming," *IEEE Trans. Signal Process.*, vol. 53, no. 5, pp. 1684–1696, May 2005.
[28] C. Zhou, "Reserch on radar countermeasures for interrupted sampling repeater jamming in time and frequency domain," Ph.D. dissertation, Dept. Elect. Eng., Beijing Inst. Technol., Beijing, China, 2018.
[29] K. Gröchenig, *Foundations of Time-Frequency Analysis*. Boston, MA, USA: Birkhäuser, 2001.
[30] Y. Qin and L.-H. Qiao, "Using ground penetrating radar time-frequency analysis methods to recognise thin-layer," in *Proc. Int. Conf. Electric Inf. Control Eng.*, Apr. 2011, pp. 5602–5604.
[31] Y. Gu and A. Leshem, "Robust adaptive beamforming based on interference covariance matrix reconstruction and steering vector estimation," *IEEE Trans. Signal Process.*, vol. 60, no. 7, pp. 3881–3885, Jul. 2010.
[32] C. Gong, L. Huang, D. Xu, and Z. Ye, "Knowledge-aided robust adaptive beamforming with small snapshots," *Electron. Lett.*, vol. 49, no. 20, pp. 1258–1259, Sep. 2013.
[33] L. Huang, X. Zhang, and Z. Ye, "Robust adaptive beamforming with a novel interference-plus-noise covariance matrix reconstruction method," *IEEE Trans. Signal Process.*, vol. 64, no. 4, pp. 1643–1650, Apr. 2015.
[34] L. Du, T. Yardibi, J. Li, and P. Stoica, "Review of user parameter-free robust adaptive beamforming algorithms," *Digit. Signal Process.*, vol. 19, no. 4, pp. 567–582, Jul. 2009.
[35] M. Barcelo, J. L. Vicario, and G. Seco-Granados, "A reduced complexity approach to IAA beamforming for efficient DOA estimation of coherent sources," *EURASIP J. Adv. Signal Process.*, vol. 2011, no. 1, Dec. 2011, Art. no. 521265.
[36] J. Li, P. Stoica, and Z. Wang, "On robust capon beamforming and diagonal loading," *IEEE Trans. Signal Process.*, vol. 51, no. 7, pp. 1702–1715, Jul. 2003.
[37] P. Chevalier and A. Blin, "Widely linear MVDR beamformers for the reception of an unknown signal corrupted by noncircular interferences," *IEEE Trans. Signal Process.*, vol. 55, no. 11, pp. 5323–5336, Nov. 2007.

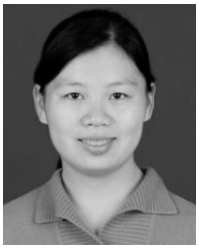

JING CHEN received the M.Eng. and Ph.D. degrees from the Xi'an University of Science and Technology, China, in 2004 and 2011, respectively. She is currently a Teacher of the School of Information and Control Engineering, Xi'an University of Architecture and Technology. Her research interests include intelligent measurement and control and industrial process and computer control.

XINLIANG CHEN was born in Hubei, China, in 1984. He received the B.E. degree in electrical science and technology from the School of Physics Science and Technology, Wuhan University, in 2005, and the Ph.D. degree from the Institute of Semiconductor, Chinese Academic of Sciences, in 2010. Since 2010, he was a Postdoctoral Researcher with the School of Information and Electronics, Beijing Institute of Technology. He joined the Beijing Institute of Technology, in 2012. His research interests include radar signal processing and radar target detection.

HONGGANG ZHANG received the Ph.D. degree from the Department of Information and Electronics, Beijing Institute of Technology (BIT), Beijing, China, in 2018. He is currently a Postdoctoral Researcher with the Department of Electronic Engineering, Tsinghua University, Beijing. His research interests include distributed array radar, wideband high resolution radar, and radar signal processing.

KAIXIANG ZHANG was born in Shanxi, China, in 1991. He received the B.S. degree from the School of Electronic Science and Technology, University of Electronic Science and Technology of China, Shandong, China, in 2015. He is currently pursuing the Ph.D. degree with the Department of Information and Electronics, Beijing Institute of Technology (BIT), Beijing, China. His research interests include distributed radar and radar signal processing.

QUANHUA LIU (Senior Member, IEEE) was born in Fujian, China, in 1982. He received the B.S. degree in telecommunications engineering from the Beijing Information Technology Institute, Beijing, China, in 2005, and the Ph.D. degree in target detection and recognition from the Beijing Institute of Technology (BIT), Beijing, in 2010. From 2010 to 2011, he was a Postdoctoral Researcher with the Antenna and Microwave Laboratory, The University of Tennessee, Knoxville, TN, USA. Since 2011, he has been a Faculty Member with BIT, where he is currently an Associate Professor. His research interests include wideband radar signal processing and distributed radar systems.